| | |
|---|---|
| ***Publication Year*** | 2015 |
| ***Acceptance in OA@INAF*** | 2020-03-20T11:01:54Z |
| ***Title*** | Enhancing the efficiency of solar concentrators by controlled optical aberrations: Method and photovoltaic application |
| ***Authors*** | GIANNUZZI, ALESSANDRA; DIOLAITI, EMILIANO; LOMBINI, MATTEO; DE ROSA, ADRIANO GIUSEPPE; MARANO, BRUNO; et al. |
| ***DOI*** | 10.1016/j.apenergy.2015.01.085 |
| ***Handle*** | http://hdl.handle.net/20.500.12386/23432 |
| ***Journal*** | APPLIED ENERGY |
| ***Number*** | 145 |

# Enhancing the efficiency of solar concentrators by controlled optical aberrations: method and photovoltaic application

Alessandra Giannuzzi[1]*, Emiliano Diolaiti[1], Matteo Lombini[1], Adriano De Rosa[2], Bruno Marano[3], Giovanni Bregoli[1], Giuseppe Cosentino[3], Italo Foppiani[1] and Laura Schreiber[1]

[1]INAF-Osservatorio Astronomico di Bologna, Via Ranzani 1, I-40127 Bologna, Italy
[2]INAF-Istituto di Astrofisica Spaziale e Fisica Cosmica, Bologna, Via P. Gobetti 101, I-40129 Bologna, Italy
[3]DIFA-Dipartimento di Fisica e Astronomia, Alma Mater Studiorum Università di Bologna, Via Ranzani 1, I-40127 Bologna, Italy

## ABSTRACT

We present a general method, based on controlled static aberrations induced in the reflectors, to boost receiver performances in solar concentrators. Imaging mirrors coupled with dense arrays suffer from severe performance degradation since the solar irradiance distribution is bell-shaped: mismatch losses occur in particular when the cells are series connected. The method consists in computing static deformations of the reflecting surfaces that can produce, for an adopted concentration ratio, a light spot matching the receiver features better than conventional reflectors. The surfaces and the deformations have been analytically described employing the Zernike polynomials formalism. The concept here described can be applied to a variety of optical configurations and collecting areas. As an example, we extensively investigated a dense array photovoltaic concentrator, dimensioned for a nominal power of about 10KWe. The "flat" distribution of light we obtain can exploit the PV device cells close to their efficiency limit. A significant gain is thus obtained, with no need of secondary optics or complex dish segmentation and of special features in the receiver electrical scheme. In the design, based on seven 2.6 m mirrors, we addressed also non-optical aspects as the receiver and the supporting mechanics. Optical and mechanical tolerances are demonstrated not to exceed accurate, but conventional, industrial standards.

**KEYWORDS**

photovoltaic concentrator (CPV), dense-array receiver, numerical optimization, optical design, Zernike polynomials

## 1. INTRODUCTION

Concentrating Photovoltaics technology (CPV) is experiencing a growing interest thanks to the development of solar cells with continuously improved efficiency. At present, the best reported cell is a 0.165 cm$^2$ multi-junction (MJ) cell having a new record of 44.4% confirmed efficiency at direct irradiance concentration of 302 suns (1 sun = 1000 W/m$^2$) [1]. For both high concentration (HCPV) and low concentration (LCPV) systems the yearly installed capacity increased significantly during the last five years [2]. A simple advantage induced by this technology is that, given the collected energy, the concentration performed by optical devices such as lenses or mirrors allows us to replace the area of photovoltaic material with cheaper optical surfaces. Moreover, high efficiency cells are too expensive to be used in non-concentrating applications. Despite most of the installed systems are point focus lens based as Fresnel [3–6] or micro-dish [7–9] systems, dense array systems have been recently investigated as profitable solutions for lowering the cost per watt-peak supplied [10, 11]. In this technology the light is focused using one large reflective element called dish, onto an array of photovoltaic MJ cells densely packed to form a single detector. If compared with lenses, mirrors have the main advantage to not suffer from chromatic aberrations. These systems track the sun in two-axis during its daily motion and usually operate in high concentration mode, i.e. with solar flux up to hundreds times the ambient value. Reflective dish concentrators with diameters ranging from few meters to few tens of meters have been already proposed and are at the beginning of their commercial development working at typical concentrations of 500× [12–14].

Traditional dish concentrators have paraboloidal shapes. Theoretically, their diameters could reach several tens of meters as the heliostats in central tower plants, the construction of monolithic mirrors being difficult at these scales. The size generally imposes to approximate the profiles with cheap flat reflecting facets mounted on a common frame and reproducing globally the paraboloidal surface. As for the receivers, standard cells have rectangular shapes and the arrays are groups of cells densely packed together mostly in series and parallels connections. The arrays do consequently resemble rectangular shapes too. When a standard imaging mirror that produces a sun image intrinsically circular is coupled with a rectangular detector problems arise. In this condition some cells could be obscured if the spot is smaller than the receiver, or part of the light could be lost if the detector is smaller than the spot, these two effects contributing to a substantial loss in efficiency. Moreover, the given irradiance distribution is bell-shaped in contrast with the requirement of having all the cells under the same illumination. In

*E-mail:alessandra.giannuzzi@unibo.it

fact, interconnected cells having identical electrical characteristics and experiencing the same irradiance/temperature conditions produce the same amount of output current and voltage. Mismatch losses occur instead when interconnected cells experience different conditions, in particular for series connections. Still few investigations have been specifically performed on current mismatches in dense array receivers exposed to high concentrations [15–17]. The issue of spatial light uniformity is instead widely known for single cell devices [18–21] and the problem is commonly approached by the introduction of secondary optics (SO) [22–24] working as homogenizers. The presence of an extra secondary optics is rather useful to increase the acceptance angle leading to a relaxation of tracking and alignment tolerances. However, this solution has the disadvantage to increase the system complexity and to add reflection losses, chromatic aberration (if refractive) and mechanical problems as alignment, stability or mounting. A useful review on the state of the art of the non-uniformity problem for single cell receivers has been recently published [25]. Few commercial systems and technical data are available on secondary optics embedded in dense arrays. Some researches faced the uniformity problem from the receiver point of view, developing new electrical connections [26], embedding different cells in the same array [27] or designing new receivers with radial symmetry [28].

Alternative ways of redesigning the primary collector have been poorly investigated but some good results has been obtained by Chong et al. [29]. The proposed planar faceted concentrator coupled to a dense array has been optimized to give a large uniform illumination over the target area with a peak intensity of 391 suns. However, such a concentrator is made by several mirrors to be mounted and aligned before being orientated with the use of line-tilting driving mechanism. Moreover, since the final spot is the overlap of the multiple facets reflections, the size and the uniformity of the final spot is influenced by projection and blocking effects which increase with the distance of the facets from the centre of the whole assembly. For this reason, such a mosaic system is not able to both have big collecting area and high concentration ratio without embedding a high number of facets and high focal distances, as reported in similar works [30–32]. In [32] the economical viability is however claimed for a specific configuration of faceted dense array system since a cost for the output power below 2 euro/watt has been calculated.

The strategy we suggest in this paper is to boost the spot uniformity by only acting on the primary reflector but using monolithic big surfaces and avoiding the dish faceting into numerous smaller elements. In the proposed method, the shape of the mirrors is analytically described by the Zernike polynomials and its optimization is numerically obtained to give a non-imaging optics able to produce a quasi-square spot, spatially uniform and with prescribed concentration. The free-form primary optics, optimized in this way and validated by a ray tracing software, showed a substantial gain in efficiency without the employ of secondary optics. At the same time, simple electrical schemes for the receiver are required. The concept has been investigated theoretically modeling a CPV application including a conceptual development of non-optical aspects as the design of the receiver and of the supporting mechanics. For the proposed method and the specific CPV system developed, a patent application has been filed in Italy. A preliminary analytical study, considering a residential utility, has been also performed in order to understand the energetic and economic performance of the system [33]. The analysis indicates that the maximum sustainable capital cost of the system ranges between 30000 euros and 45000 euros depending on the years which are considered for the return of the investment (10 or 20 years respectively). Further more detailed economical evaluations will be performed during the future constructive phases of the project.

## 2. Optical Concept

From an optical point of view there is no need for an accurate image at the receiver of a solar concentrator. The optical design criteria rather concern with the optimal transfer of light between the source and the target chosen. To solve matching issues in concentrators we thought to reinterpret optical concepts largely used in astronomy, where an accurate image formation is an essential premise for efficient observations. In telescopes, controlled mirrors deformations are introduced by actuators to balance the optical aberrations that degrade the wavefront coming from an observed source [34–36]. What we developed instead is a sort of "reverse" approach of the astrophysical method: the guideline is to apply deformations (active or static) to the mirrors of the solar collectors to introduce aberrations in the wavefront, thus degrading the solar image and, in the case of a CPV dense array system, focusing a squared spot with a prescribed irradiance. The result would be a better match between the irradiance features and the receiver performance.

The technical feasibility of our concept is supported by independent studies and projects involving technology transfer processes from the astronomical instrumentation knowledge. Single monolithic reflectors suitable for concentrators (3.1 meter wide) have been already realized in a customized furnace at the Steward Observatory Mirror Lab, at the University of Arizona [37]. A novel mirror concept based on an active laminate consisting of an ultra-thin (less than 1 mm) and ultra-light carbon-fiber shell bonded to a piezo-ceramic active layer have been recently investigated and manufactured with the aim of reducing the cost of active mirrors both in telescopes and concentrators [38–40].

To describe the mirrors shape and to perform the optimization for a CPV dish, we used the *Zernike polynomials*, an analytical tool largely employed, especially in optics, to characterize functions and data on a circular domain. They form an orthogonal basis on the unit circle and real surfaces can be represented by linear combinations of them. Every Zernike polynomial consists of three components: a normalization factor, a radial component and an azimuthal component. The radial components are polynomials derived from

the Jacobi polynomials, whereas the azimuthal component is sinusoidal. As in the Noll formalism [41], the Zernike polynomials can be defined in polar coordinates $(\rho, \theta)$:

$$Z_{j_{even}} = \sqrt{n+1} R_n^m \rho \sqrt{2} \cos m\theta \quad (1)$$

$$Z_{j_{odd}} = \sqrt{n+1} R_n^m \rho \sqrt{2} \sin m\theta \quad (2)$$

$$Z_j = \sqrt{n+1} R_n^0(\rho) \quad (3)$$

where $\rho$ is the normalized radial coordinate ranging from 0 to 1 and $\theta$ is the azimuthal angle ranging from 0 to $2\pi$. In the formulas, $m$ represents the azimuthal frequency and $n$ the radial degree, both are integer and the condition $m \leq n$, $n - |m| =$ even must be satisfied. The index $j$ is a mode ordering number and is a function of $n$ and $m$. Equations 1 and 2 exist for $m \neq 0$ while equation 3 for $m = 0$. The double indexing scheme is useful for unambiguously describing the functions. In the formulas, $R_n^m(\rho)$ indicates polynomials with radial dependence.

## 3. Case of single on-axis mirror

An analysis we performed with the ray tracing software Zemax® showed that, starting from a spherical mirror, very few deformations described by specific Zernike polynomials (modes) can strongly help in solving the uniformity and shape problem in dense array receivers. Considering an imaging mirror with deformations, its surface $z$ (the so-called *sag*) can be approximated by the following formula:

$$z = \frac{cr^2}{1 + \sqrt{1 - (1+k)c^2r^2}} + \sum_{i=1}^{N} A_i Z_i(\rho, \theta) \quad (4)$$

where $N$ is the number of polynomials, $A_i$ is the coefficient associated to the $i^{th}$ polynomial, $r$ is again the radial coordinate in the chosen units, $\rho$ and $\theta$ are the polar coordinates defined before. Eq. 4 depends on the curvature $c$ (which equals the reciprocal of the curvature radius) and the conic constant $k$. The first term in the equation represents an ideal conic surface (spherical if $k = 0$) while the second term represents the deformations described by Zernike polynomials. The number of terms needed for a good surface modeling grows together with the number of deformations occurring at different scales.

| Zernike Mode | | |
|---|---|---|
| 4th | 11th | 14th |
| 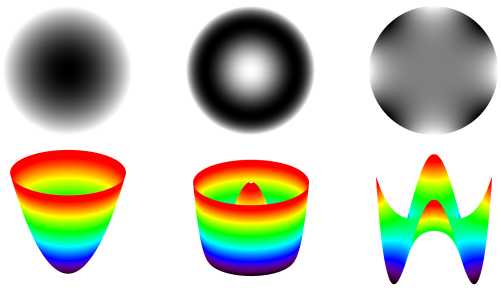 | | |

**Table 1:** Principal Zernike modes involved in this study.

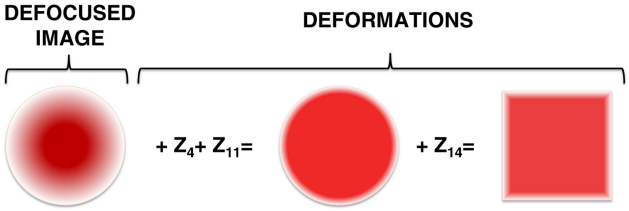


**Figure 1:** Effects introduced on the Sun image by Zernike polynomials 4th, 11th and 14th

For a single spherical mirror focusing on axis, we identified three main polynomials: the 4th, the 11th and the 14th. Fig. 1 shows how the solar spot produced at a fixed distance by a spherical mirror can be modified by introducing controlled deformations related to the three modes here mentioned. This model can be also extended to mirrors with an off-axis focus: in that case the number of Zernike modes involved in the spot shaping is higher.

The identified modes are shown in 2D and 3D in Table 1. The deformation associated with the 4th mode (*defocus*) basically enlarges the image and contributes to spread the light quite similarly to the effect of shifting the receiver plane. The 11th mode (*third order spherical*) contributes to redistributing the rays maintaining an image radial symmetry and changing the image irradiance profile. These two polynomials do not have any impact on the spot shape since they have no azimuthal dependence. A deformation corresponding to the 14th polynomial (*vertical quadrafoil*) contributes to make a circular spot square along two preferential directions rotated 45 degree, depending on the coefficient sign. The effect of this specific deformation is less evident if the mirror is in focus mode: that is the reason for a combined use of the modes 14th and 4th. Alternatively, the same effect of this combination can be obtained by positioning the receiver slightly behind or above the correct focal plane and avoiding (partially or completely) the deformations related to the 4th mode. Since it is easier for a single mirror to produce a square uniform image when the defocus is bigger, this means that the lower the concentration factor the better the method works. The size of the spot to obtain depends on the desired concentration factor.

A prescribed irradiance could be also obtained by employing this concept to design concentrators with several optimized mirrors focusing at the same receiver. In this case, the final illumination pattern impinging on the receiver would result in the sum of the incoherent illumination patterns produced by each single mirror, as we are going to show in the next sections.

## 4. Case of a CPV dense array system: design choices

A multi-mirror configuration can be useful to solve the issue of building a single huge mirror. In order to avoid a mosaic of hundreds reflective elements [15], we choose to design a CPV dish made by few monolithic mirrors mounted close together on the same structure. The selected configu-

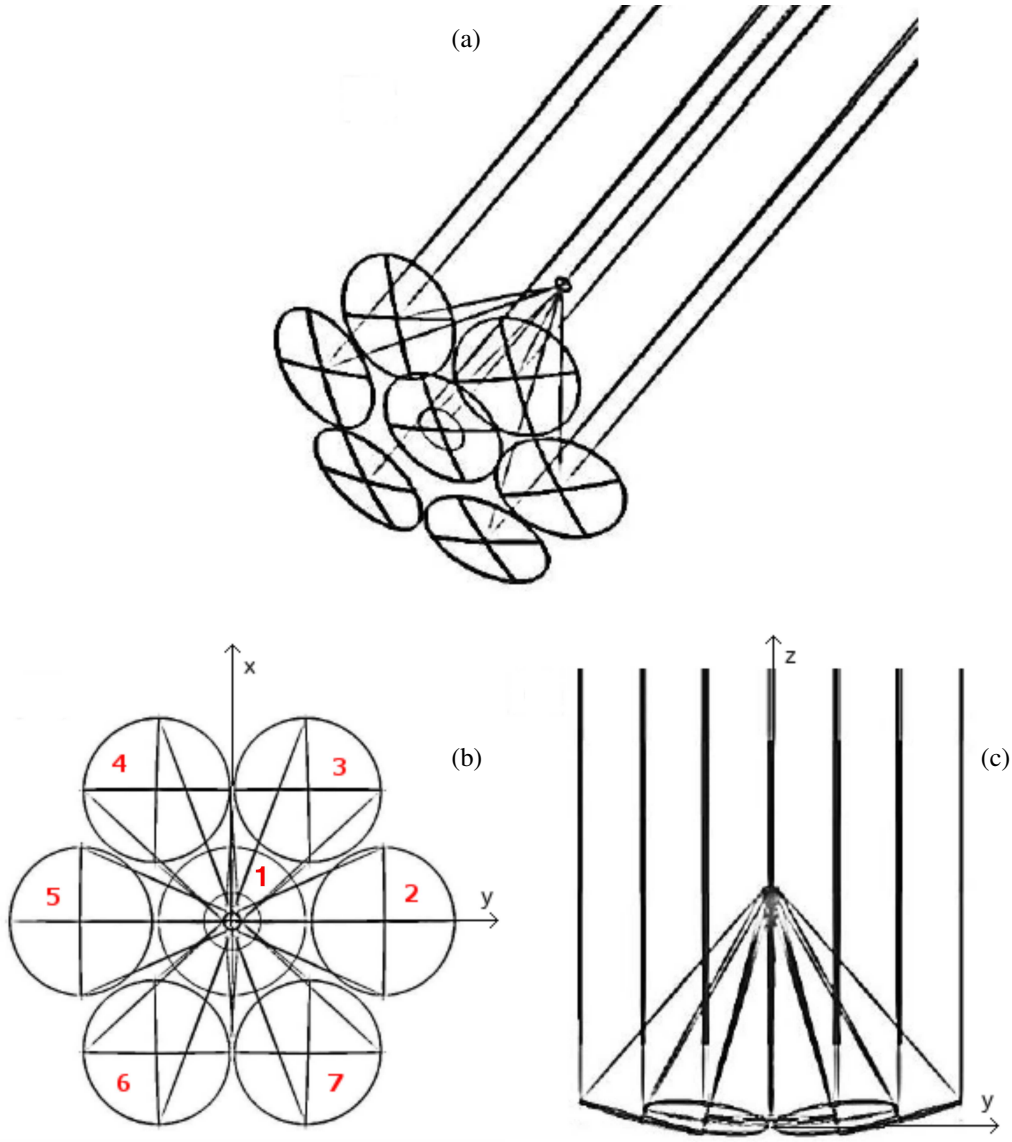


**Figure 2:** Optical layouts: a) 3D, b) x-y plane, c) y-z plane.

ration is the hexapolar grid and it has been already used in Stirling applications as well as in some ground based optical telescopes. In the hexapolar configuration the elements are placed on rings so that the (n+1)$^{th}$ ring contains six elements more than the n$^{th}$ ring, the central ring having only one element. We decided to consider only the central mirror and a ring of six mirrors arranged around it. Figure 2 presents the optical layouts of the proposed system. The mirrors of the second ring have been labeled from 2 to 7 counter-clockwise. The z-axis has been set as the direction of the incoming rays and it is perpendicular to the central mirror vertex. This optical condition of alignment with the solar direction should be the system nominal working state.

Considerations about the concentration ratio to be investigated and the mechanical compactness have been made also in comparison with similar existing prototypes and plants. Since this research activity has been carried out with the specific goal of finding new solutions in the field of clean micro-generated distributed electricity, our dish has been conceived as a power system suitable for the market of medium residential contexts or small farms. We decided the mirror diameter to be around 2-3 meters, to avoid construction difficulties. The diameter of the single mirror has been set to $D = 2600$ mm, for a total system size of about 7800 mm and a resulting total optical area slightly bigger than 35 m$^2$. Supposing an irradiance at the collecting aperture of 1000 W/mm$^2$, the entry power would be around 35 KW: with a receiver working almost at the efficiency of the best presently available cells (between 30%-40%), such a system would be able to deliver more than 10 KWe. Utility scale applications could be anyway considered, together with the scaling of the single elements for higher energy outputs.

The detector distance has been set to $h = 4800$ mm in order to have a low ratio of detector distance to total diameter. Considering this ratio similar to the focal ratio in imaging systems, a value $f/0.5$ should be approached to maximize

| | Mirr1 | Mirr2 | Mirr3 | Mirr4 | Mirr5 | Mirr6 | Mirr7 |
|---|---|---|---|---|---|---|---|
| **X pos** (mm) | 0.00 | 0.00 | 2320.88 | 2320.88 | 0.00 | -2320.88 | -2320.88 |
| **Y pos** (mm) | 0.00 | 2680.00 | 1340.00 | -1340.00 | -2680.00 | -1340.00 | 1340.00 |
| $\alpha_{\mathbf{x}}(^\circ)$ | 0.00 | -14.59 | -7.41 | 7.41 | 14.59 | 7.41 | -7.41 |
| $\alpha_{\mathbf{y}}(^\circ)$ | 0.00 | 0.00 | 12.60 | 12.60 | 0.00 | -12.60 | -12.60 |
| **radius of curv.** (mm) | 10101.00 | 11480.10 | 11480.10 | 11480.10 | 11480.10 | 11480.10 | 11480.10 |

**Table 2:** Positions, tilt angles and curvatures of the seven mirrors.

the concentration but also to allow a more compact structure.

We investigated two concentration levels, 500× and 800×. To obtain these concentrations, we applied a defocus to the mirrors which is the common method to modulate the concentration delivered at the receiver. A paraboloid in focus mode would have a collected flux too high for the cells working range (up to few thousands of suns at present). In our case, another reason to avoid extreme concentrations is that the deformations introduced by the Zernike modes are more efficient in reproducing the image features required when a defocus occurs.

The concentrator has been initially designed putting mirrors with the same diameter $D$ on the same plane. The reference system has been chosen so that incoming rays are parallel to the z-axis, while the mirrors vertexes lay in the x-y plane. Each mirror has been placed at $d = 2680$ mm (in the x-y plane) from the central mirror vertex to prevent shading effects. The mirrors of the external ring have been tilted respect to the central one in order to focus all the chief rays from the Sun center at the center of the receiver plane having coordinates $(0, 0, h)$. This optical restriction is optional, but we aimed at simplifying the mechanical structure. The geometrical laws fulfilling this optical condition are easily derivable and once fixed the distance $d$ in the hexapolar grid the positional/tilting parameters of the mirrors can be immediately calculated. The tilt of the external mirrors reduce by 5% the collecting projected area of the whole system from 37.17 $m^2$ to about 35.25 $m^2$. Positions, tilts and curvatures of the seven mirrors are listed in Table 2. The generic mirror surface sag has been described by Eq. 4.

## 5. Design Method

To optically model our system, an end-to-end IDL® code has been written on purpose. Each step of the procedure and the results have been verified with the optical design software Zemax® as reference. The code includes four main subgroups of routines: the first for individually modeling the optical part; the second for the receiver implementation; the third for optimizing the optics; the last one for calculating tolerances of optical/mechanical parameters.

### 5.1 Optical Modeling

The initial optical parameters, which are the initial conditions of the simulations, have been set by a ray tracing analysis performed by Zemax®. The Sun has been modeled as a finite source with an angular diameter of $0.53°$, neglecting its shape variations caused by the altitude changing during the day. The curvatures have been set so that the mirrors could produce a spot with a size compatible with the mean geometrical concentration chosen. The concentration ratio has been defined as the total mirrors area perpendicular to the axis of the central mirror divided by the total area of the receiver, supposing a receiver and a spot ideally with the same size. We ignored the obscuration introduced by the receiver itself.

The Zernike modes corresponding to deformations useful to fulfill our requirements of shape and uniformity have been selected after fixing the curvature. The deformations needed for the central mirror are the three described in paragraph 2, but other modes (from $5^{th}$ to $8^{th}$) are necessary for the six off-axis mirrors. The selection criteria is that the superimposition of all the generated spots could produce an irradiance distribution with the desired features. Symmetry properties have been imposed for the six mirrors in the external ring to reduce the degrees of freedom of our problem. For example, these mirrors have been chosen with the same curvature radius and the same values of the $4^{th}$, $11^{th}$ and $14^{th}$ Zernike coefficients. As consequence, the non-zero coefficients are linked between mirrors by the geometrical relations shown in Table 3. In this way, opposite mirrors are equal but rotated by $\pi$ and the final optical model results to be made of only four different types of surfaces. It could be certainly possible to identify more coefficients to improve the performance however increasing the complexity of the system. This condition would be more suitable both on construction and calibration stages. The independent modes identified for our system are eight, three for the central mirror (Z4(1), Z11(1) and Z14(1)) and five for the external ones, all derived from the modes of the mirror number 2 (Z4(2), Z6(2), Z7(2), Z11(2), Z14(2)) according to the relations shown in Table 3. The mirrors of the ring can not have all the same shapes even if this would be the best constructive condition. The $14^{th}$ Zernike mode in fact corresponds to a deformation able to modify the circular symmetry of the ray bundle into a square and it has an azimuthal dependence. The simple rotation of a given surface would lead to a different analytical description in terms of its Zernike coefficients, except for the coefficients with pure radial dependence. This means that a ring generated by replicating mirror number 2 and simply rotating the replicas according to the position in the ring, would give a series of identical spot rotated as in Fig. 3a. The superimposition of these spots would certainly not lead

| | Mirr1 | Mirr2 | Mirr3 | Mirr4 | Mirr5 | Mirr6 | Mirr7 |
|---|---|---|---|---|---|---|---|
| **Z4** | Z4(1) | Z4(2) | Z4(2) | Z4(2) | Z4(2) | Z4(2) | Z4(2) |
| **Z5** | 0.00 | 0.00 | -Z6(2)$\cdot \cos 30°$ | Z6(2)$\cdot \cos 30°$ | 0.00 | -Z6(2)$\cdot \cos 30°$ | Z6(2)$\cdot \cos 30°$ |
| **Z6** | 0.00 | Z6(2) | -Z6(2)$\cdot \sin 30°$ | -Z6(2)$\cdot \sin 30°$ | Z6(2) | -Z6(2)$\cdot \sin 30°$ | -Z6(2)$\cdot \sin 30°$ |
| **Z7** | 0.00 | Z7(2) | Z7(2)$\cdot \sin 30°$ | -Z7(2)$\cdot \sin 30°$ | -Z7(2) | -Z6(2)$\cdot \sin 30°$ | Z7(2)$\cdot \sin 30°$ |
| **Z8** | 0.00 | 0.00 | Z7(2)$\cdot \cos 30°$ | Z7(2)$\cdot \cos 30°$ | -Z7(2) | -Z6(2)$\cdot \cos 30°$ | -Z7(2)$\cdot \cos 30°$ |
| **Z11** | Z11(1) | Z11(2) | Z11(2) | Z11(2) | Z11(2) | Z11(2) | Z11(2) |
| **Z14** | Z14(1) | Z14(2) | Z14(2) | Z14(2) | Z14(2) | Z14(2) | Z14(2) |

**Table 3:** Correlation between the Zernike coefficients of the seven mirrors.

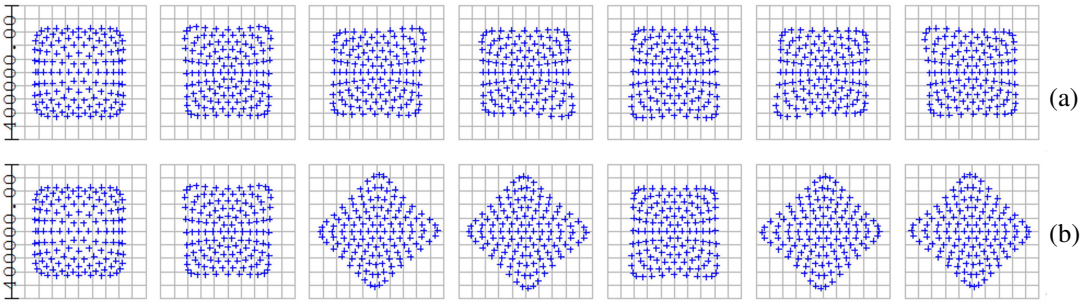


**Figure 3:** Effect introduced in the spot generated by each mirror by the introduction of a) a Z14 value rotated according to the mirror location and b) a common Z14 value.

to a final square shape. On the contrary, fixing the 14$^{th}$ coefficient to the same value for all the surfaces, the features in Fig. 3b are obtained. The physical size of the figure is $4 \cdot 10^5$ µm.

The optical scheme described is simulated by the ray-tracing code written on purpose. The code output is the final spot produced by the concentrator. In the algorithm, the continuous optical surfaces of the mirrors have been discretized by a fixed number of sub-apertures. The rays striking every sub-aperture are reflected toward the receiver according to the classic reflection law. The Sun has been modeled as an homogeneous circular source with a diameter of 0.53°, thus applying a realistic divergence model. The number of rays traced from the Sun has been set in order to minimize sampling errors. To calculate the nominal mirrors shape, we supposed an ideal tracking condition in which the central solar ray strikes the central mirror vertex parallel to the optical axis.

| | |
|---|---|
| **Base Material** | GaInP/GaAs/Ge on Ge substrate |
| **AR Coating** | TiOx/Al2Ox |
| **Chip size** | 5,59 x 6,39 mm$^2$= 35.25 mm$^2$ |
| **Active Cell Area** | 5,5 x 5,5 mm$^2$=30,25 mm$^2$ |

**Table 4:** Main features of the AZUR SPACE 3C40 cell implemented in the simulations.

## 5.2 Receiver Implementation

To simulate the performance of a dense array receiver, we considered an electrical model for the PV cells. Neglecting any temperature or spectral variation, the physical behavior of a cell can be in first approximation summarized by the following set of equations uniquely depending on the concentration factor $\times$:

$$I_{sc}(\times) = \times \cdot I_{sc}(1) \tag{5}$$

$$V_{oc}(\times) = V_{oc}(1) + n_d \frac{KT \ln(\times)}{q} \tag{6}$$

$$P_{max}(\times) = I_{max}(\times) \cdot V_{max}(\times) \tag{7}$$

$$FF(\times) = \frac{P_{max}(\times)}{I_{sc}(\times) \cdot V_{oc}(\times)} \tag{8}$$

$$\eta_{max}(\times) = \frac{P_{max}(\times)}{P_{in}(\times)} = I_{sc}(\times) \cdot V_{oc}(\times) \cdot \frac{FF(\times)}{P_{in}(\times)} \tag{9}$$

where $P_{in}$ is the total power received by the cell and $I_{sc}(\times)$, $V_{oc}(\times)$ are short circuit current and open circuit voltage at a given concentration, $\eta_{max}$ is the nominal conversion efficiency, $n_d$ is the diode ideality factor, $T$ is the absolute temperature of the cell, $K$ is the Boltzmann constant and $q$ is the electron charge. A more exhaustive model involving dependences on $T$ and spectral variations can be found in [42]. Equation 8 defines the Fill Factor $FF$ as the ratio between the power at the maximum power point $P_{max}$ and the product of the open circuit voltage and short circuit current. It is typically better than 75% for good quality MJ solar cells. It is also an index of the performance of a solar cell in terms of generated power and it should be as close as possible to 100%: graphically, the $FF$ is a measure of the *squareness* of the solar cell $I-V$ curve and is also the area of the largest rectangle which would fit in the curve.

Our receiver has been analytically designed and numerically simulated using a datasheet of commercially available high concentration cells 3C40 produced by AZUR SPACE

| | $\mathbf{I_{sc}}$(A) | $\mathbf{V_{oc}}$(V) | $\mathbf{I_{max}}$(A) | $\mathbf{V_{max}}$(V) | $\mathbf{P_{max}}$(W) | **FF**(%) | $\boldsymbol{\eta}$(%) |
|---|---|---|---|---|---|---|---|
| **500**× | 2.151 | 3.144 | 2.102 | 2.842 | 5.98 | 88.0 | 39.0 |
| **1000**× | 4.239 | 3.170 | 4.135 | 2.762 | 11.42 | 85.0 | 37.8 |

**Table 5:** Electrical parameters of the AZUR SPACE 3C40 cell at 500× and 1000×.

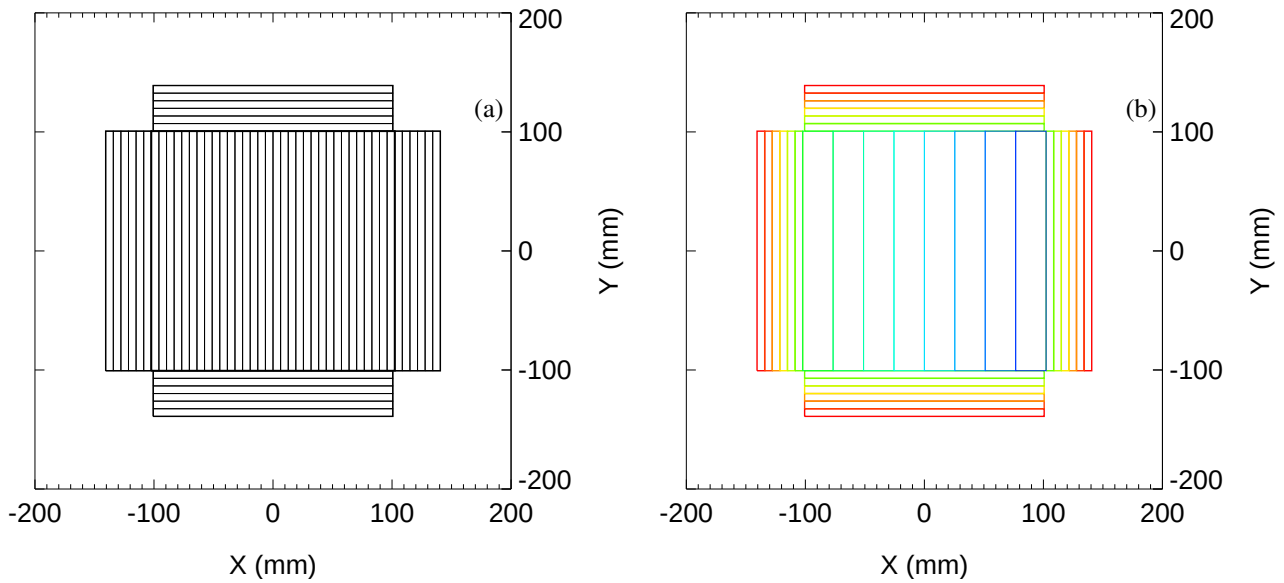


**Figure 4:** Type-3 receiver design at 500×. The a) panel shows the subdivision in strings. The b) panel shows which strings are series connected (zones with the same color). The 14 resulting blocks are parallel connected.

[44] with a nominal efficiency of 39% at 500× (around 38% at 1000×) at ambient temperature. The reference cell has main features described in Table 4.

In addition to efficiency, the cell datasheet gives other output parameters (Table 5) necessary in the simulations to predict the cells power output at different illuminations. Moreover, since we deal exclusively with reflective elements, no chromatic aberration are introduced. The temperature can also be considered reasonably constant as efficient cooling systems have been shown in literature.

The receiver electrical design has been chosen in order to minimize the *power matching* problem even maintaining high degree of linearity and easiness of construction: attention has been paid to series connected cells since the output current in this case corresponds to the current produced by the worst illuminated cells of the series.

The choice of the number of cells to connect has been made starting from the concept that a receiver should have a certain area to perform at a certain mean concentration. The array design has to resemble, with the right connections, an irradiance distribution which is mostly square and uniform and probably degrading toward the borders. To simplify the scheme, we decided to simulate different receivers starting from the same base unit, which is a string of series connected cells. A scheme with many parallels would lead to a lower dependence from irradiance gradients, but it has the inconvenience to give high current and small voltages in output. High voltages are instead more suitable for the standard range of inverters while small currents limit the resistive losses. We thus chose to conceptually design different receivers type to perform at different output voltages. Figures 4a and 4b shows the third of the array implemented for which we will show also the tolerance results. It is a detector made by 56 strings of 36 cells. The strings spatial positioning is shown in Fig. 4a where each string is represented by a narrow rectangle. There are 32 strings in the central square zone, which corresponds roughly to the maximum uniform area obtainable by the optimization, and 4 lateral zones made by 6 additional modules each. The total number of cells is 2016. This scheme allows cells in series to be irradiated with similar fluxes and at the same time, the strings and the groups contain the same number of elements thus ensuring small parallel mismatches. This scheme does not have cells at the corners, since the spillage losses in case of 500× have been evaluated in the order of 5%. The electrical connections are arranged as follows (Fig. 4b): cells in each strings are series connected as well as strings with the same color. The central zone is then made by 8 blocks of cells each containing 4 adjacent substrings (the subdivision of each colored areas have been omitted), while the lateral strings are series connected in concentric frames. The 14 resulting blocks are finally parallel connected.

The same electrical scheme has been also used for simulating the concentration 800×. In this case the cells of the base string are only 27 and the central zone is made by 24 strings since the higher concentration results in a smaller ir-

radiated area. The parallel connected blocks are 12. Spillage losses at the corners are around 8-10% but again we preferred to preserve the array symmetry avoiding cells in these areas.

To analytically calculate the electrical performance, we developed a routine implementing the equations (5)-(9) modeling the cell output current and voltage as functions of concentration, neglecting resistive effects. As for the electrical scheme, the routine implements the classical equations for calculating voltages and currents in series and parallel connections. Only these connections are involved while no model has been implemented for the bypass diodes. A temperature of $T = 298$ K has been considered and a reasonable value for the ideality factor $n_d = 3.3$ has been assumed to treat the junctions as real. The other initial parameters used are in Table 5. Being $FF$ only dependent on $V_{oc}$, it has been calculated using a classical empirical formula [43] approximated for zero resistivity:

$$FF(\times) = \frac{v_{oc}(\times) - \ln(v_{oc}(\times) + 0.72)}{1 + v_{oc}(\times)} \tag{10}$$

where $v_{oc}(\times)$ is the open circuit voltage normalized by the factor $n_d KT/q$.

## 5.3 Optimization procedure

The optimization procedure employs a downhill simplex method. We decided to minimize a merit function related to conversion efficiency. In particular it has been defined as the negative efficiency of the receiver $-\eta$ as defined in Eq. 9: each evaluation of this function requires the calculation of the efficiency by the ray tracing procedure and the receiver model previously explained. We summarize the optimization steps as follows.

The initial values chosen for the parameters to be optimized are inserted in the optimization routine. The routine operates performing a multidimensional minimization of a function $func(x)$ where $x$ is an n-dimensional vector of parameters, using a downhill simplex method requiring only function evaluations and not derivatives. Additional input for the routine are the fractional tolerance to be achieved in the function value as well as the range of the parameters variation.

The optimization procedure transfers the parameters value to the ray-tracing procedures which gives the image as output, then the block simulating the receiver performance gets in input the image focused by the optics. The image is represented by a matrix containing the local concentration impinging on each receiver cell. The receiver model distinguishes between cells series and parallel connected, imposing the current of a series cells as the current produced by the worst illuminated cell. Subsequently, the current and voltage output for each series/parallel are summed to give the total output and the efficiency. After calculating the efficiency of the optics coupled with that receiver, the procedure changes the parameters value iteratively in the range specified, modifying the optics and calculating a new image, a corresponding new efficiency and comparing the values of the simplex obtained. When the minimum is found within the threshold, the routine returns an n-element vector corresponding to the function minimum value. This kind of method could be applied to other type of receivers and it could be improved by extending the variables (for example the curvatures that here we considered fixed).

## 5.4 Tolerance calculation

After obtaining the nominal image produced by the optimized optics, a tolerance calculation has been implemented to assess the feasibility of the results. Tolerances have been obtained for both optical and geometrical parameters. We considered 25 parameters for each of the 4 different mirrors. Additional parameters are the two tracking angles and the receiver position along the z-axis, for overall 178 parameters. The parameters include tilts and positions of the mirrors, their curvatures and the Zernike coefficients up to the $6^{th}$ radial order (from $4^{th}$ to $21^{th}$). The reason for considering up to this order lays in the connection between the radial degree of the polynomials and the spatial scale of the deformations: the degree of a polynomial on a certain surface (which has a diameter of 2.6 m in the proposed design) roughly defines the spatial scale (period) of the associated deformation so that, for example, a $6^{th}$ degree deformation on 2.6 m diameter would be roughly half meter ($2.6/6$ m$= 0.43$ m). It has been evaluated that higher degree deformations, i.e. occurring on spatial scales smaller than the considered scale, can be reasonably controlled by surface polishing of candidate materials (aluminum, molded plastics, etc.). The tolerances have been also calculated for polynomials with nominal null coefficients since all the polynomials up to a certain degree are necessary to model the irregularities down to a given scale.

The nominal image produced by the optics with the optimized parameters and the corresponding receiver efficiency have been calculated and stored as terms of comparison. We chose a range of variation for each parameter and a minimum tolerable efficiency. The tolerated efficiency degradation was equally split among all the parameters, assuming their effects as uncorrelated. Degraded efficiency has been calculated for the minimum and maximum values of a given parameter, keeping nominal values for all the other parameters: if the degraded efficiency is acceptable, the minimum

| | **Z4(1)** | **Z11(1)** | **Z14(1)** | **Z4(2)** | **Z6(2)** | **Z7(2)** | **Z11(2)** | **Z14(2)** |
|---|---|---|---|---|---|---|---|---|
| **500**× | 1.124 | 0.137 | 0.098 | 1.486 | -0.616 | 0.223 | 0.003 | -0.217 |
| **800**× | 1.103 | 0.070 | -0.108 | 1.053 | -0.714 | 0.280 | 0.019 | -0.144 |

**Table 6:** Values in mm of the Zernike coefficients optimized at the two considered concentrations considering type-3 receivers.

and maximum values of the given parameter are adopted as tolerances for that parameter, otherwise the variation range of the parameter is reduced and the process is repeated until convergence. After computing the tolerances for each parameter separately, the global effect has been evaluated by perturbing all the parameters simultaneously in a random fashion according to the computed tolerances and evaluating the corresponding efficiency.

## 6. RESULTS: THE SOLARIS CONCENTRATOR

The results shown in Table 6 have been obtained by optimizing our optics at two concentrations (500× and 800×) with type-3 receivers. The values of the Zernike coefficients not shown can be derived from the relations in Table 3.

The bi-dimensional and the x-cross section irradiance produced by the optimized optics have been simulated by Zemax® for the two concentration ratios and they are shown in Fig. 5 and Fig. 6. The x-cross section irradiance is evaluated on the central row parallel to the x-axis of the bi-dimensional irradiance pattern. All the simulations have been performed supposing 1 sun irradiance at the concentrator aperture, which is the common value in Standard Test Conditions (STC).

The performance obtained for other receivers types described in Section 5.2 are listed in Table 7. The efficiency $\eta$ is the output power of the receiver divided by the total power collected by the optics. The optimized systems show a conversion efficiency of about 30% in all the cases with 500× and of 28% in the only analysed case with 800×. The case with higher concentration is interesting for the development of new generation cells because it shows that the proposed method gives good results also at higher concentrations. Moreover, the higher the concentration the smaller the number of cells employed in the receiver. The case with concentration 800× in fact includes only 1152 cells, almost half of the cells needed for the concentration 500× (2016 elements).

The relative efficiency $\eta_{rel}$ in Table 7 has been defined considering the only effective power impinging on the array, i.e. accounting for spillage losses at the corners/edges. This parameter is useful to evaluate the average cells performance in the array. In three of the four cases, its value is above 31% and it must be compared with the maximum theoretical efficiency reported in Section 5.2 for the active part of the cell considered, i.e. 33% for concentration 500× and 32% for 1000×. This means that the cells in the arrays work really close to their nominal performance under the irradiance produced by the optimized optics.

Looking at the results in Table 7 with concentration 500×, the main difference between the three receivers analyzed lays in the output parameters values. Even if the total power produced is quite similar in all the cases (slightly higher than 10 KWe), the output current and voltage are very different. The third receiver has been designed specifically with a high number of series connections to obtain a high voltage value (409.2 V) suitable for the available inverters and with small current (25.3 A) to limit the resistive losses. This condition is convenient from an electrical point of view, but it leads to tighter tolerances, as shown below.

The tolerance results are here shown only for the concentration 500× with the type-3 receiver, giving some qualitative indications for the other cases studied. The parameters which differ from mirror to mirror are summarized in Tables 8 and 9 while the common parameters related to the receiver position are shown in Table 10. Five out of seven mirrors have been omitted from the list since their tolerances are similar to those of the second mirror except for discretization effects. The last row in Table 8 is the root square sum (RSS) of the Zernike coefficients and it is one of the most important tolerance indicators in our analysis since it represents the tolerated surface sag deviation. For all the mirrors, this parameter is in the order of tenths of a millimeter. The shape deviation tolerated is also compatible with the manufacturing irregularities of candidate materials (molded plastics or aluminum) for the deformed/deformable mirrors. The tracking errors shown in Table 10 are quite small if compared to other CPV concentrators (normally in the order of 1 milliradian or more). In any case, the tracking accuracy can be achievable with standard tracking solutions commonly employed in telescopes since these systems can also reach subarcseconds tolerances. Good pointing and active tracking systems are already developed also for solar concentrators [45], but their performances should be further improved to allow our tolerances.

The calculations have been performed setting a threshold of 3% on the efficiency, i.e. tolerating a degradation of the performance from 29.4% down to 26.4%. This value has been chosen as reasonable for this type of systems, but it can be varied depending on the required performance. In general, for small perturbations, the tolerance on a parameter scales linearly with the threshold value. The tolerances are strictly related to the electrical scheme implemented in the receiver. For example we calculated that with the receiver involving more parallels and with the same threshold, the tolerances would be three times more relaxed. In that case higher output current would be produced, the output power being approximately the same.

The mechanical model is shown in Fig. 7. From the analysis of the Zernike polynomials, the desired deformations on the mirrors can be applied by a restricted number of actuators positioned on a certain number of control points. For the system with the chosen dimensions, these points are located radially on three circumferences every 10°. A possible way to obtain the final surfaces is to use spherical mirrors and to set the deformations by the actuators. Another approach is to freeform mirrors already shaped with the final form desired, the actuators being employed only to compensate the shape errors once the mirrors have been placed on their own support. All these mirrors could be made by aluminum sheets, since this material is particular suitable for its lightness and its ductility. Molded plastic could be also a candidate substrate material (if compatible with the requested tolerances) after the deposition of a high reflective layer. During the

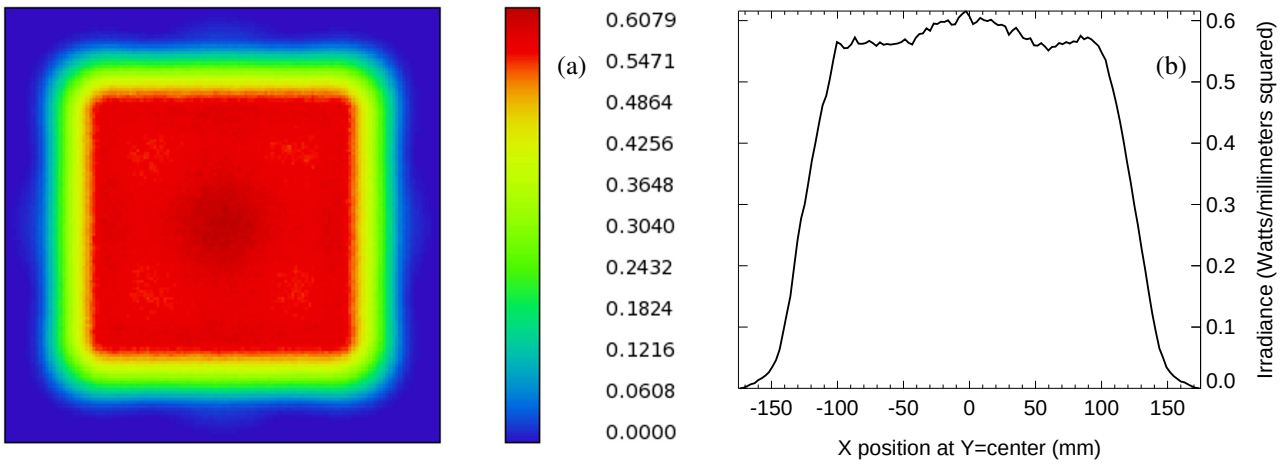


**Figure 5:** a) 2D and b) x-cross section irradiance produced by the optics coupled to the type-3 designed for 500×. The physical size of the figures is 350 mm. Units in the color bar are Watt/mm$^2$.

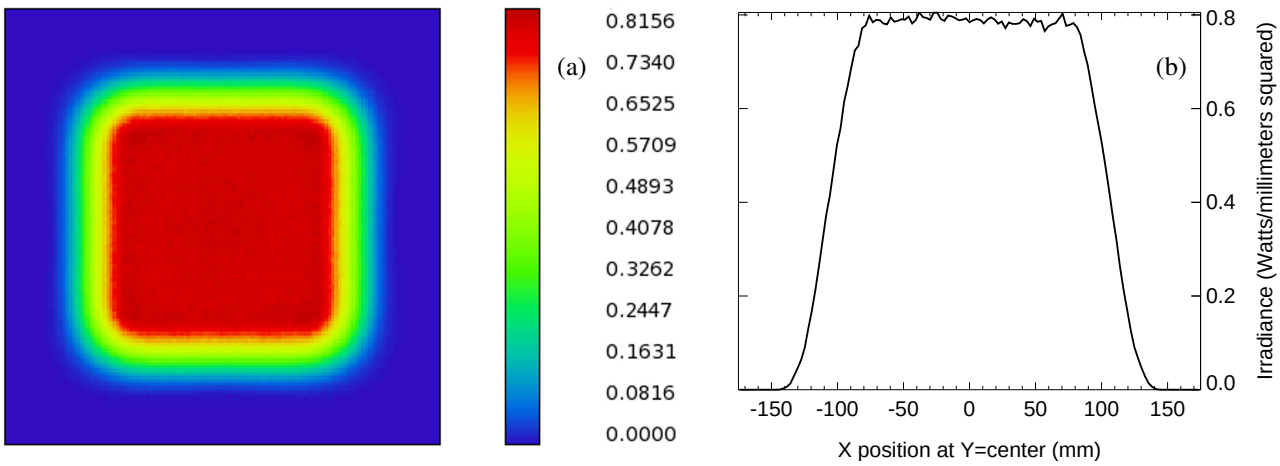


**Figure 6:** a) 2D and b) x-cross section irradiance produced by the optics coupled to the type-3 designed for 800×. The physical size of the figures is 350 mm. Units in the color bar are Watt/mm$^2$.

| | $\mathbf{I_{out}}$(A) | $\mathbf{V_{out}}$(V) | $\mathbf{P_{out}}$(W) | $\eta$(%) | $\eta_{\mathbf{rel}}$(%) |
|---|---|---|---|---|---|
| **Receiver 1** (500×) | 98.7 | 105.2 | 10288.0 | 29.2 | 30.5 |
| **Receiver 2** (500×) | 50.5 | 204.6 | 10324.8 | 29.7 | 31.6 |
| **Receiver 3** (500×) | 25.3 | 409.2 | 10354.5 | 29.4 | 31.2 |
| **Receiver 3** (800×) | 32.6 | 302.6 | 9868.1 | 28.0 | 31.4 |

**Table 7:** Electrical performance obtained after the optimization run with the three receivers implemented.

| Units | Parameter | Mirr1 | | Mirr2 | |
|---|---|---|---|---|---|
| | | nominal value | tolerance | nominal value | tolerance |
| | **Z4** | 1.124 | 0.063 | 1.486 | 0.063 |
| | **Z5** | 0.000 | 0.063 | 0.000 | 0.031 |
| | **Z6** | 0.000 | 0.250 | -0.616 | 0.063 |
| | **Z7** | 0.000 | 0.031 | 0.223 | 0.016 |
| | **Z8** | 0.000 | 0.031 | 0.000 | 0.016 |
| | **Z9** | 0.000 | 0.031 | 0.000 | 0.031 |
| | **Z10** | 0.000 | 0.031 | 0.000 | 0.016 |
| | **Z11** | 0.137 | 0.008 | 0.003 | 0.016 |
| | **Z12** | 0.000 | 0.016 | 0.000 | 0.008 |
| **mm** | **Z13** | 0.000 | 0.016 | 0.000 | 0.008 |
| | **Z14** | 0.098 | 0.016 | -0.217 | 0.031 |
| | **Z15** | 0.000 | 0.016 | 0.000 | 0.016 |
| | **Z16** | 0.000 | 0.016 | 0.000 | 0.004 |
| | **Z17** | 0.000 | 0.004 | 0.000 | 0.008 |
| | **Z18** | 0.000 | 0.016 | 0.000 | 0.008 |
| | **Z19** | 0.000 | 0.008 | 0.000 | 0.008 |
| | **Z20** | 0.000 | 0.016 | 0.000 | 0.016 |
| | **Z21** | 0.000 | 0.016 | 0.000 | 0.008 |
| **mm** | $\sqrt{\sum \mathbf{Z^2}}$ | | **0.2762** | | **0.1122** |

**Table 8:** Zernike coefficients tolerances calculated for the system with 500× coupled with a type-3 receiver.

| Units | Parameter | Mirr1 | | Mirr2 | |
|---|---|---|---|---|---|
| | | nominal value | tolerance | nominal value | tolerance |
| **mm** | **radius of curv.** | 10101.0 | 25.0 | 11480.1 | 25.0 |
| | **tilt x** | 0.0 | 0.4 | -254.6 | 0.2 |
| **mrad** | **tilt y** | 0.0 | 0.9 | 0.0 | 0.1 |
| | **tilt z** | 0.0 | 1.7 | 0.0 | 1.7 |
| | **offset x** | 0.0 | 5.0 | 0.0 | 2.5 |
| **mm** | **offset y** | 0.0 | 2.5 | 2680.0 | 2.5 |
| | **offset z** | 0.0 | 25.0 | 0.0 | 3.1 |

**Table 9:** Tolerances on other parameters calculated for the system with 500× coupled with a type-3 receiver.

realization, the system should be aligned within tolerances. For this reason, we conceived a 2-step procedure. The first phase consists in the mirrors positioning on their own supports and the calibration of their nominal shape. This test can be performed in laboratory and it requires a point light source, a beam splitter, a Shack-Hartmann (SH) wavefront sensor [46] with a camera. The camera acquires the image of a point source reflected back by the mirror which can be used to recognize the wavefront shape and the mirror surface map. The actuators are tuned iteratively until the measured surface map matches its nominal value (within tolerances, see Tables 9 and 10). To accelerate the calibration procedure, an interaction matrix records the SH sensor reaction to the specific movement of each single actuator. This matrix has to be inverted and used to transform the SH sensor signal into incremental corrections to apply to the actuators. The second stage is an alignment on Sun of each mirror on the whole frame. A mask dimensioned as the receiver and realized in a material resistant to temperatures of a few hundreds degrees is needed. Concentric frames of pinholes on the mask transmit part of the light impinging on the receiver plane to diodes or other electronic light-sensitive devices. Such a tool allows to sample the irradiance distribution produced by the optics and to adjusted iteratively the position of each mirror on the common frame until the desired irradiance is obtained. Another interaction matrix is used to record the diodes reaction to the parameters to align. This matrix is then inverted and used to translate the measured signal into corrections for the mirror positioning.

The new concentrator resulting from the investigation carried out has been called "SOLARIS (SOLAR Image Squaring) Concentrator" and it has been patented in Italy. The patent is owned by both the University of Bologna and the National Institute of Astrophysics (INAF), the two research institutes involved in the project. Main subjects of the patent are both the innovative concentrating CPV application and the method for the numerical optimization of reflective surfaces. The procedures to test/calibrate the reflective shapes and to align the mirrors on Sun, as well as the receiver and the mechanical design are all parts of the patent. The model

| Units | Parameter | All Mirrors | |
|---|---|---|---|
| | | nominal value | tolerance |
| **mrad** | **tracking error x** | 0.0 | 0.11 |
| | **tracking error y** | 0.0 | 0.01 |
| **mm** | **receiver offset z** | 4800.0 | 2.5 |

**Table 10:** Tolerances calculated for to the common parameters.

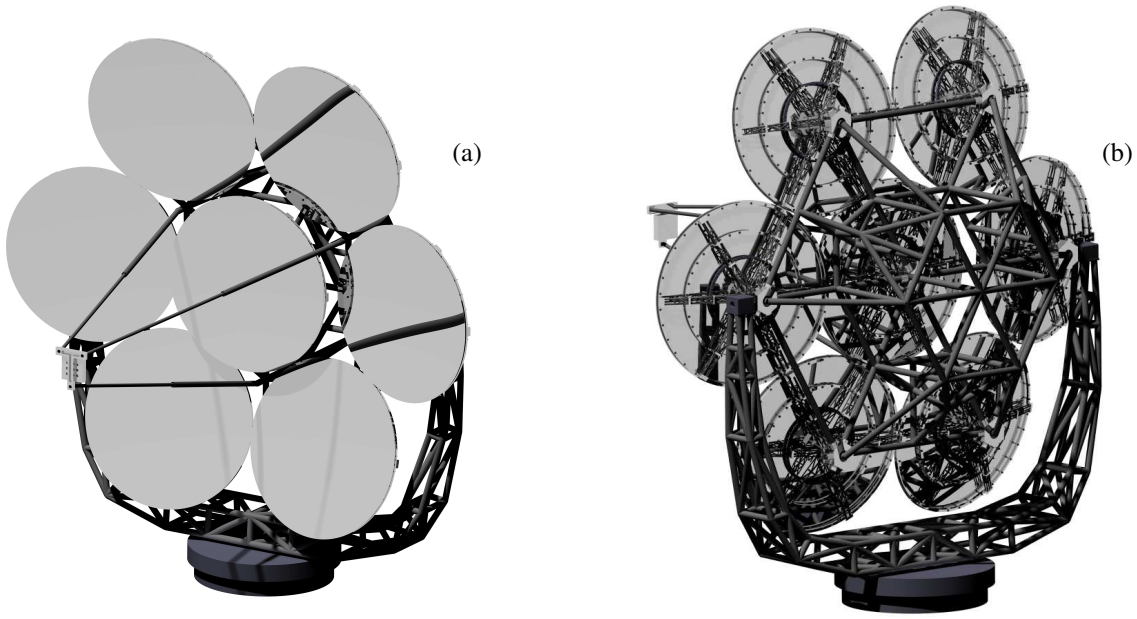


**Figure 7:** Shaded models of the SOLARIS Concentrator: a) front side, b) rear side.

and the obtained results will be validated with the described procedures during the forthcoming prototyping stage.

## SUMMARY AND DISCUSSION

We developed a new optical designing method for solar concentrators. In particular, dense array photovoltaic applications need an accurate control on both shape and irradiance of the collected light spot to perform at high efficiency. These systems are experiencing in the last years growing interest (from market and research) as feasible solutions in the production of cost competitive electricity on demand, especially in very sunny environments and off-grid communities. The development of solar cells that can work at very high irradiance imposes a technological jump also from an optical point of view, to let these systems work at the same performance of the employed cells. The proposed method is based on controlling the optical shapes so that the spot produced by the mirrors can resemble the optimal features for the chosen receiver without including secondary optics. The deformations to apply have been analytically modelled by the Zernike polynomials and the deformed mirrors have been simulated by ray tracing routines developed on purpose. At the same time, different schemes of dense array receivers have been designed using reference cells with known features and simulated by implementing simple electrical models for photovoltaic devices. The deformed optics have been numerically optimized to maximize the performance of the concentrator as a function of the coupled receiver. The method has been fruitfully employed to solve the prescribed irradiance problem at high concentration in CPV dishes. It has led to the design of a novel CPV optics, the SOLARIS concentrator. Both the method implemented and the specific application developed have been patented in Italy.

The main advantage of using big monolithic mirrors is to have few optics to manage respect to the complex segmented optics proposed in other researches involving dense arrays. Despite this technology is quite recent and commercial plants are not as diffused as the refractive fresnel lens based systems, our method to design dense array concentrators opens a new scenario for developing PV systems that could perform at very high efficiency working at high concentrations. This efficiency boosting up to nominal levels and, at the same time, the relaxation of the constraints on the receiver design and the recent development of new materials for optical application suggest interesting perspectives of cost reduction.

The concentrator developed is a single stage multi-mirror system made by 7 monolithic optics placed in an hexapolar arrangement and all focusing on the same receiver. The principal investigated design has a mean concentration ra-

tio 500×. The deformations applied to the optics allow them to produce a solar spot resembling a square shape with smoothed corners. The irradiance pattern inside the spot obtained is highly uniform. At this concentration, the optimized optics can boost the conversion efficiency of the whole receiver up to 30%, almost the same theoretical performance of the single cell used in the calculations which is around 33% (considering only the active areas). The receiver has been designed as simple as possible, using exclusively strings of identical cells in series. The strings are then organized in parallels or series connections, with a Cartesian configuration and not involving bypass diodes in the design.

From an optical point of view, different considerations can been made to extend the purposes and the applications of the method conceived. Similar systems with different concentrations can be surely designed ever keeping in mind the optimization method has been tested for the two concentration 500× and 800×, and that the results are better in the first case considered thanks to the higher defocus involved. Despite this, we demonstrated that our method can work efficiently also at many hundreds of concentration ratio.

Method improvements could be done by a further investigation of the convenient deformations to introduce, exploring for example the effects related to Zernike polynomials of higher degrees. The selected deformations and the optical configuration used in this work are indeed only an example of the method proposed: other concentrators could be designed by adding deformations or changing the geometrical/optical parameters as a function of the desired spot features. Systems with single or multiple mirrors (different or not) could be implemented and different geometrical configurations explored. Also the mirrors aperture could be varied in shape and size depending on the amount of output power needed or on the economical/constructive constraints. The final spot could result from a superimposition of images not necessarily centered in the same point, as in the studied cases. Another interesting application could result form exploring the performance of deformable optics including very simple reflective secondary optics to recover possible light losses at the receiver borders or to relax the tolerances (thus enhancing the acceptance angle).

A great advantage of employing actively deformable optics could be given by the tuning of the concentration ratio. Using convenient deformable materials, flexible systems could be obtained embedding different type of receivers but exploiting the same optics. Also from the receiver point of view, great improvements could be obtained in terms of electric efficiency, involving optimized electrical schemes or thinking to future monolithic receivers. Finally, an extension of this method could be also helpful in solving thermal problems. Thermal concentrators do also need a certain uniformity in the light collected to optimally transfer the energy to the exchanging fluid. The proposed technique could be implemented to correct possible optical aberrations thus boosting the concentration up to its limit.

## ACKNOWLEDGEMENTS

This research activity has been financially supported by a MIUR PhD grant and a Fondazione CARISBO grant within the research framework on renewable sources, energy spare and distributed micro-generation.

## REFERENCES

[1] Green MA, Emery K, Hishikawa Y, Warta W, Dunlop ED. Solar cell efficiency tables (version 42). *Prog. Photovolt: Res. Appl.* 2013; **21**: 827-837. doi:10.1002/pip.2404

[2] Wiesenfarth M, Helmers H, Philipps SP, Steiner M, Bett AW. Advanced concepts in concentrating photovoltaics (CPV). *Proc. of 27th European Photovoltaic Solar Energy Conference and Exhibition* 2012, Frankfurt, Germany: 11-15. doi:10.4229/27thEUPVSEC2012-1AP.1.4

[3] Benítez P, Miñano J, Zamora P, Mohedano R et al. High performance Fresnel-based photovoltaic concentrator. *Opt. Express* 2010; **18**: A25-A40. doi:10.1364/OE.18.000A25

[4] Singh PL, Sarviya RM, Bhagoria JL. Thermal performance of linear Fresnel reflecting solar concentrator with trapezoidal cavity absorbers. *Applied Energy* 2010; **87**(2): 541-550. doi:10.1016/j.apenergy.2009.08.019

[5] Ryu K, Rhee JG, Park KM, Kim J. Concept and design of modular Fresnel lenses for concentration solar PV system, *Solar Energy* 2006,; **80**(2): 1580-1587. doi:10.1016/j.solener.2005.12.006

[6] Leutz R, Suzuki A, Akisawa A, Kashiwagi T. Design Of A Nonimaging Fresnel Lens For Solar Concentrators. *Solar Energy* 1999; *65*(6): 379-387. doi:10.1016/S0038-092X(98)00143-1

[7] Feuermann D, Gordon J. High-concentration photovoltaic designs based on miniature parabolic dishes. *Solar Energy* 2001; **70**(5): 423-430. doi:10.1016/S0038-092X(00)00155-9

[8] Kribus A, Kaftori D, Mittelman G, Hirshfeld A et al. A miniature concentrating photovoltaic and thermal system. *Energy Conversion and Management*; **47**(20): 3582-3590. doi:10.1016/j.enconman.2006.01.013

[9] Gordon JM, Katz EA, Eugene A, Feuermann D, Mahmoud H. Toward ultrahigh-flux photovoltaic concentration. *Applied Physics Letters* 2004; **84**: 3642-3644. doi:10.1063/1.1723690

[10] http://www.apollon-eu.org

[11] Kinsey GS, Sherif RA, Cotal HL, Pien P et al. Multijunction Solar Cells for Dense-Array Concentrators. *Proc. of the IEEE 4th World Conf. on Photovoltaic Energy Conversion* 2006: 625-627. doi:10.1109/WCPEC.2006.279532

[12] Verlinden P, Lewandowski A, Bingham C, Kinsey G, Sherif R, Lasich J. Performance and Reliability of Multijunction III-V Modules for Concentrator Dish and Central Receiver Applications. *Proc. of the IEEE 4th World Conf. on Photovoltaic Energy Conversion* 2006: 592-597. doi:10.1109/WCPEC.2006.279526

[13] Chayet H, Kost O, Moran R, Lozovsky I. Efficient, Low Cost Dish Concentrator for a CPV Based Cogeneration System. *AIP Conference Proceedings* 2011; **1407**: 249-252. doi:10.1063/1.3658337

[14] Lasich JB, Verlinden PJ, Lewandowski A, Edwards D et al. World's first demonstration of a 140kWp Heliostat Concentrator PV (HCPV) system. *34th IEEE Photovoltaic Specialists Conference (PVSC)* 2009: 002275,002280. doi:10.1109/PVSC.2009.5411354

[15] Chong KK, Siaw FL. Electrical Characterization of Dense-Array Concentrator Photovoltaic System. *27th European Photovoltaic Solar Energy Conference* 2012; Frankfurt, Germany. doi:10.4229/27thEUPVSEC2012-1AV.3.18

[16] Minuto A, Timo G, Groppelli P, Sturm M. Concentrating photovoltaic multijunction (CPVM) module electrical layout optimisation by a new theoretical and experimental mismatch analysis including series resistance effect.*35th IEEE Photovoltaic Specialists Conference (PVSC)* 2010; 003081-003086. doi:10.1109/PVSC.2010.5614540

[17] Cooper T, Pravettoni M, Cadruvi M, Ambrosetti G, Steinfeld A. The effect of irradiance mismatch on a semi-dense array of triple-junction concentrator cells. *Solar Energy Materials and Solar Cells* 2013; **116**: 238-251. doi:10.1016/j.solmat.2013.04.027

[18] Luque A, Sala G, Arboiro JC. Electric and thermal model for non-uniformly illuminated concentration cells. *Solar Energy Materials and Solar Cells* 1998; **51**(3-4): 269-290. doi:10.1016/S0927-0248(97)00228-6

[19] Franklin E, Coventry J. Effects of highly non-uniform illumination distribution on electrical performance of solar cells. *Proc. Solar Australian and New Zeeland Solar Energy Society* 2003

[20] Katz EA, Gordon JM, Feuermann D. Effects of ultra-high flux and intensity distribution in multi-junction solar cells. *Prog. Photovolt: Res. Appl.* 2006; **14**(4): 297-303. doi:10.1002/pip.670

[21] Herrero R, Victoria M, Domínguez C, Askins S, Antón I , Sala G. Concentration photovoltaic optical system irradiance distribution measurements and its effect on multi-junction solar cells. *Prog. Photovolt: Res. Appl.* 2012; **20**(4): 423-430. doi:10.1002/pip.1145

[22] Hernández M, Cvetkovic A, Benítez P, Miñano JC. High-performance Kohler concentrators with uniform irradiance on solar cell. *Proc. SPIE 7059, Nonimaging Optics and Efficient Illumination Systems V* 2008; n.705908. doi:10.1117/12.794927

[23] Fu L, Leutz R, Annenn HP. Evaluation and comparison of different designs and materials for Fresnel lens-based solar concentrators. *Proc. SPIE 8124, Nonimaging Optics: Efficient Design for Illumination and Solar Concentration VIII* 2011; n.81240E. doi:10.1117/12.893390

[24] Leutz R, Suzuki A, Akisawa A, Kashiwagi A. Flux uniformity and spectral reproduction in solar concentrators using secondary optics. *ISES Solar World Congress* 2001; Adelaide

[25] Baig H, Heasman KC, Mallick TK. Non-uniform illumination in concentrating solar cells. *Renewable and Sustainable Energy Reviews* 2012; **16**(8): 5890-5909. doi:10.1016/j.rser.2012.06.020

[26] Salemi A, Eccher M, Miotello A, Brusa RS. Dense array connections for photovoltaic systems. *Prog. Photovolt: Res. Appl.* 2011; **19**(4): 379-390. doi:10.1002/pip.1040

[27] Loeckenhoff R, Kubera T, Rasch KD. Water Cooled TJ Dense Array Modules for Parabolic Dishes. *AIP Conference Proceedings* 2010; **1277**: 43-46. doi: 10.1063/1.3509229

[28] Vivar M, Antón I, Sala G. Radial CPV receiver. *Prog. Photovolt: Res. Appl.* 2010; **18**(5): 353-362. doi: 10.1002/pip.921

[29] Chong KK, Wong CW, Siaw FL, Yew TK. Optical Characterization of Nonimaging Planar Concentrator for the Application in Concentrator Photovoltaic System. *J. Sol. Energy Eng* 2010; **132**(1) n. 011011. doi:10.1115/1.4000355

[30] Siaw FL, Chong KK, Wong CW. A comprehensive study of dense-array concentrator photovoltaic system using non-imaging planar concentrator. *Renewable Energy* 2014; **62**: 542-555. doi: 10.1016/j.renene.2013.08.014

[31] Riveros-Rosas D, Sánchez-González M, Arancibia-Bulnes CA, Estrada CA. Influence of the size of facets on point focus solar concentrators. *Renewable Energy* 2011; **36**(3): 966-970. doi:10.1016/j.renene.2010.08.038

[32] Tan MH, Chong KK, Wong CW. Optical characterization of nonimaging dish concentrator for the application of dense-array concentrator photovoltaic system. *Appl. Opt.* 2014; **53**(3): 475-486. doi:10.1364/AO.53.000475

[33] Bianchi M, Diolaiti E, Giannuzzi A, Marano B, Melino F. Energetic and Economic Analysis of a New Concept of Solar Concentrator for Residential Application. *Energy Procedia, in Proc. of the 7th International Conference on Applied Energy ? ICAE* 2015; Abu Dhabi, United Arab Emirates

[34] Wilson RN, Franza F, Noethe L. Active Optics I: A system for optimizing the optical quality and reducing the costs of large telescopes. *Journal of Modern Optics* 1987; **34**(4): 485-509

[35] Noethe L, Franza F, Giordano P, Wilson RN et al. Active Optics II. Results of an Experiment with a Thin 1 m Test Mirror. *Journal of Modern Optics* 1988; **35**(9): 1427-1457. doi:10.1080/09500348814551591

[36] Biasi R, Gallieni D, Salinari P, Riccardi A, Mantegazza P. Contactless thin adaptive mirror technology: past, present, and future. *Proc. SPIE - Adaptive Optics Systems II* 2010; 7736. doi:10.1117/12.858816

[37] Angel R, Connors T, Davison W, Olbert B, Sivanandam S. New architecture for utility-scale electricity from concentrator photovoltaics. *Proc. of SPIE - The International Society for Optical Engineering* 2010; 7769

[38] Steeves J, Pellegrino S. Ultra-Thin Highly Deformable Composite Mirrors. *54th AIAA/ASME/ASCE/AHS/ASC Structures, Structural Dynamics, and Materials Conference* 2013

[39] Ning X, Pellegrino S. Design of lightweight structural components for direct digital manufacturing. *53rd AIAA/ASME/ASCE/AHS/ASC Structures, Structural Dynamics and Materials Conference* 2012

[40] Irschik H. A review on static and dynamic shape control of structures by piezoelectric actuation. *Engineering Structures* 2002; **24**(1): 5-11. doi:10.1016/S0141-0296(01)00081-5

[41] Noll R. Zernike polynomials and atmospheric turbulence. *J. Opt. Soc. Am.* 1976; **66**(3): 207-211. doi:10.1364/JOSA.66.000207

[42] Domínguez C, Antón I, Sala G. Multijunction solar cell model for translating I-V characteristics as a function of irradiance, spectrum, and cell temperature. *Prog. Photovolt: Res. Appl.* 2010; **8**(4): 272-284. doi:10.1002/pip.965

[43] Green MA. Solar cell fill factors: General graph and empirical expressions. *Solid-State Electronics* 1981; **24**(8): 788-789. doi:10.1016/0038-1101(81)90062-9

[44] http://www.azurspace.com

[45] Fontani D, Sansoni P, Francini F, Jafrancesco D et al. Pointing sensors and sun tracking techniques. *International Journal of Photoenergy* 2011; n. 806518. doi:10.1155/2011/806518

[46] Shack RV, Platt BC. Production and use of a lenticular Hartmann screen. *J. Opt. Soc. Am.* 1971; **61**(5): 656-660.